Effect of the electron gas polarizability on the specific heat of phonons in Coulomb crystals

D. A. Baiko
A. F. Ioffe Physical–Technical Institute, 194021 St. Petersburg, Russia

(Received 1 September 2001; revised manuscript received 4 September 2002; published 15 November 2002)

The effect of the background polarizability on the thermodynamic properties of a Coulomb crystal of ions is studied. The response of electrons is treated using the Thomas-Fermi (TF) and random phase approximations (RPA). For the case of ions fixed at their lattice sites, the energy of bcc and fcc crystals is calculated to first order in the screening parameter $(\kappa_{\rm TF}a)^2$ ($\kappa_{\rm TF}$ is the TF wave number and a is the ion sphere radius). It is shown that in the RPA there exist domains of parameters (mass density ρ and charge number Z) where energy of fcc crystal is lower than that of bcc. The effect of ion vibrations is studied using harmonic lattice approximation. It is shown that phonon modes are nearly identical in the RPA and in the TF approximation. The latter allows one to apply the Ewald technique to the construction of the dynamical matrix, which speeds up all calculations considerably. The main thermodynamic quantities of phonons are calculated as functions of the quantum parameter T_p/T (where T_p is the ion plasma temperature) and the screening parameter. The electron polarizability leads to a moderate increase of the phonon thermodynamic quantities as compared to the case of one-component plasma with rigid background (by $\sim$30% at $\kappa_{\rm TF}a=0.8$). Zero-point motion of ions modifies the aforementioned domains where fcc has lower energy than bcc for static ions. The effect is profound at small Z but leaves the domains unaltered at larger Z. The thermal vibrations of ions at $T\gtrsim T_p$ eliminate completely the domains where fcc is thermodynamically preferable at $T=0$. The related model of Yukawa-Wigner solid is briefly studied. It is shown that neither bcc nor fcc crystal structures are stable in this model.

DOI: 10.1103/PhysRevE.66.056405 PACS number(s): 52.27.Lw, 52.27.Gr

I. INTRODUCTION

It is well known that the model of one-component plasma (OCP) of ions is not entirely appropriate for the description of matter in the deep, fully ionized layers of white dwarf cores or neutron star crusts. In fact, the electron gas, forming the background that compensates the electric charge of ions, possesses finite polarizability and therefore screens pure Coulomb potential of ions. Obviously, this modifies various properties of the system as compared to the case of OCP.

The effect of the electron gas polarizability has been studied in a number of works for solid and liquid plasma of ions within the framework of the linear response formalism (e.g., Refs. [1–4], and references therein). The linear response formalism assumes that the screening parameter $\kappa_{\rm TF}a<1$, where $\kappa_{\rm TF}$ is the Thomas-Fermi (TF) wave number (to be defined later), while $a=(3/4\pi n)^{1/3}$ is the ion sphere radius (n is the number density of ions). Generally, the response of electrons is described by the dielectric function evaluated using the random phase approximation (RPA).

In parallel to the above work, a series of papers has appeared (e.g., Ref. [5], and references therein) devoted to the study of the so-called Yukawa-Wigner Solid (YWS). The YWS is a crystal of point charges immersed into the compensating charged background distributed as $(\kappa^2/4\pi)e^{-\kappa|\mathbf{R}-\mathbf{r}|}/|\mathbf{R}-\mathbf{r}|$ around each lattice point $\mathbf{R}$, κ being the inverse screening length. The normalization coefficient is chosen in such a way that the overall charge of the background associated with given point charge compensates fully the point charge. The results reported in Ref. [5] are valid for an arbitrary value of the screening parameter κa. The same distribution of background charges occurs if one takes the OCP as the undisturbed system (system of ''external'' charges) and sets $\epsilon(q)=1+\kappa^2/q^2$, where $\epsilon(q)$ is the longitudinal dielectric function at energy transfer $\omega=0$, and q is the momentum transfer. The RPA static longitudinal dielectric function behaves as $1+\kappa_{\rm TF}^2/q^2$ at small q.

The aim of the present paper is to give some new results on the YWS, to make a connection between the two approaches to the treatment of the screening, to check the extent to which the results on the YWS are appropriate for matter in the interior layers of the degenerate stars, and to present new calculations of thermodynamic properties (energy, specific heat, etc.) of Coulomb crystals with the polarizable electron background in the linear response framework.

II. STATIC LATTICE ENERGY

Consider Coulomb plasma of ions with charge number Z and polarizable background of nearly free degenerate electrons compensating the total charge. In the linear response formalism, the energy per ion, E, for a system of N ions fixed at some spatial points $\mathbf{X}$ in a volume V at temperature $T=0$ reads (e.g., Ref. [2])

$$E=E_0+U, \tag{1}$$

$$\frac{U(\{\mathbf{X}\})}{Z^2e^2}=\frac{1}{2NV}\sum_{\mathbf{X}\neq\mathbf{X}'}\sum_{\mathbf{q}\neq0}\frac{4\pi}{q^2\epsilon(q)}e^{i\mathbf{q}(\mathbf{X}-\mathbf{X}')}+\frac{1}{2V}\sum_{\mathbf{q}\neq0}\frac{4\pi}{q^2}\left[\frac{1}{\epsilon(q)}-1\right], \tag{2}$$

where E_0 is the kinetic energy of the ideal degenerate electron gas and $U(\{\mathbf{X}\})$ is the correction due to Coulomb interaction. The thermodynamic limit $N\to\infty$ is implicitly assumed for all intensive quantities. If ions form a lattice, and

are fixed at their lattice sites $\mathbf{X}=\mathbf{R}$ (the static lattice case), Eq. (2) can be considerably simplified:

$$\frac{U}{Z^2e^2}\equiv\frac{U(\{\mathbf{R}\})}{Z^2e^2}$$
$$=\frac{1}{2}\sum_{\mathbf{R}}{}'\int\frac{d\mathbf{q}}{(2\pi)^3}\frac{4\pi e^{i\mathbf{q}\cdot\mathbf{R}}}{q^2\epsilon(q)}$$
$$+\frac{1}{2}\int\frac{d\mathbf{q}}{(2\pi)^3}\frac{4\pi}{q^2}\left[\frac{1}{\epsilon(q)}-1\right]$$
$$-\frac{n}{2}\int d\mathbf{r}\int\frac{d\mathbf{q}}{(2\pi)^3}\frac{4\pi e^{i\mathbf{q}\cdot\mathbf{r}}}{q^2\epsilon(q)}. \tag{3}$$

Here, the sum goes over all lattice vectors $\mathbf{R}$, excluding the $\mathbf{R}=0$. U includes the electrostatic (Madelung) energy of the OCP [which corresponds to $\epsilon(q)\equiv1$] and the first-order correction due to electron polarization. Formally, since $\epsilon(q)$ is in the denominator, we have all powers of the quantity $\epsilon(q)-1$, but only the lowest-order term is described correctly [Eq. (2) itself is valid only within the linear formalism framework]. Notice that we neglect exchange and correlation energy of electrons. However, as explained in the end of this section, Eq. (3) includes change of electron kinetic energy due to Coulomb interactions with ions.

To begin with, consider the TF form of the dielectric function which is a useful approximation in various problems and which describes also the screening in the YWS. In this case we have

$$\epsilon_{\mathrm{TF}}(q)=1+\frac{\kappa_{\mathrm{TF}}^2}{q^2},\quad \kappa_{\mathrm{TF}}=2k_{\mathrm{F}}\sqrt{\frac{e^2}{\pi\hbar v_{\mathrm{F}}}}, \tag{4}$$

where k_{F} and v_{F} are the Fermi momentum and velocity of electrons. In this approximation, one can apply the Ewald technique to the lattice sum in Eq. (3), with the result

$$\frac{U_{\mathrm{TF}}}{Z^2e^2}=\sum_{\mathbf{R}}{}'\frac{1}{4R}(E_++E_-)+\sum_{\mathbf{G}}\frac{2\pi n}{G^2+\kappa_{\mathrm{TF}}^2}e^{-A(G^2+\kappa_{\mathrm{TF}}^2)}$$
$$-\frac{2\pi n}{\kappa_{\mathrm{TF}}^2}-\frac{e^{-A\kappa_{\mathrm{TF}}^2}}{2\sqrt{\pi A}}-\frac{\kappa_{\mathrm{TF}}}{2}\mathrm{erf}(\kappa_{\mathrm{TF}}\sqrt{A}). \tag{5}$$

In this case, $\mathbf{G}$ is a reciprocal lattice vector, while A is an arbitrary constant chosen to optimize both (direct and reciprocal) lattice sums;

$$E_\pm=e^{\pm\kappa_{\mathrm{TF}}R}\mathrm{erfc}\left(\frac{R}{2\sqrt{A}}\pm\kappa_{\mathrm{TF}}\sqrt{A}\right), \tag{6}$$

and $\mathrm{erfc}(x)=1-(2/\sqrt{\pi})\int_0^x dt e^{-t^2}$ for any real x. From Eq. (5) we recover the well-known expression for the Madelung energy in the limit $\kappa_{\mathrm{TF}}=0$:

$$\frac{U_{\mathrm{M}}}{Z^2e^2}=\frac{1}{2}\sum_{\mathbf{R}}{}'\frac{1}{R}\mathrm{erfc}\left(\frac{R}{2\sqrt{A}}\right)+\sum_{\mathbf{G}}{}'\frac{2\pi n}{G^2}e^{-AG^2}-\frac{1}{2\sqrt{\pi A}}$$
$$-2\pi nA. \tag{7}$$

Let us remind the values of $\zeta=U_{\mathrm{M}}/(Z^2e^2/a)$ for body-centered-cubic (bcc) and face-centered-cubic (fcc) crystals:

$$\zeta_{\mathrm{bcc}}=-0.895\,929\,255\,682,$$
$$\zeta_{\mathrm{fcc}}=-0.895\,873\,615\,195. \tag{8}$$

In the next order in κ_{TF}^2, we get $U_{\mathrm{TF}}-U_{\mathrm{M}}=U_{1\mathrm{TF}}+\ldots$ with

$$\frac{U_{1\mathrm{TF}}}{Z^2e^2}=\kappa_{\mathrm{TF}}^2\left\{\frac{1}{4}\sum_{\mathbf{R}}{}'\left[R\,\mathrm{erfc}\left(\frac{R}{2\sqrt{A}}\right)-2\sqrt{\frac{A}{\pi}}e^{-R^2/4A}\right]\right.$$
$$\left.+\pi nA^2-\frac{1}{2}\sqrt{\frac{A}{\pi}}-2\pi n\sum_{\mathbf{G}}{}'\frac{e^{-AG^2}}{G^2}\left(A+\frac{1}{G^2}\right)\right\}. \tag{9}$$

Writing $U_{1\mathrm{TF}}=\eta(\kappa_{\mathrm{TF}}a)^2Z^2e^2/a$, we have

$$\eta_{\mathrm{bcc}}=-0.103\,732\,333\,707,$$
$$\eta_{\mathrm{fcc}}=-0.103\,795\,687\,531. \tag{10}$$

These numbers are in good agreement with the corresponding coefficient $\eta_{\mathrm{liq}}=-0.1032$ (e.g., Ref. [2]) in the expansion of the energy of the strongly coupled Coulomb liquid; the latter is obtained by numerical integration using accurate liquid structure factor in the TF model.

The correction to the Madelung energy for an arbitrary dielectric function $\epsilon(q)$ reads

$$\frac{U_1}{Z^2e^2}=\frac{1}{2}\sum_{\mathbf{R}}\int\frac{d\mathbf{q}}{(2\pi)^3}\frac{4\pi e^{i\mathbf{q}\cdot\mathbf{R}}}{q^2}\left[\frac{1}{\epsilon(q)}-1\right]$$
$$-\frac{1}{2}\int d\mathbf{r}\int\frac{d\mathbf{q}}{(2\pi)^3}\frac{4\pi e^{i\mathbf{q}\cdot\mathbf{r}}}{q^2}\left[\frac{1}{\epsilon(q)}-1\right]$$
$$=\sum_{\mathbf{G}}{}'\frac{2\pi n}{G^2}\left[\frac{1}{\epsilon(G)}-1\right]\approx-\sum_{\mathbf{G}}{}'\frac{2\pi n}{G^2}[\epsilon(G)-1]. \tag{11}$$

In this case,

$$\eta=-\frac{3}{2}\sum_{\mathbf{G}}{}'\frac{\epsilon(G)-1}{(Ga)^2(\kappa_{\mathrm{TF}}a)^2}. \tag{12}$$

According to Jancovici [6], the RPA dielectric function of the relativisitc electron gas at $T=0$ is

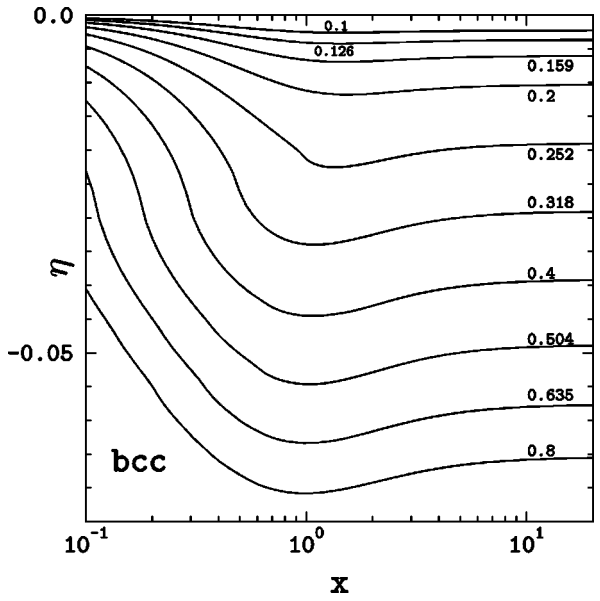

FIG. 1. Quantity η, Eq. (12), for bcc lattice as a function of x for ten values of $\kappa_{\mathrm{TF}}a$, indicated near the curves.

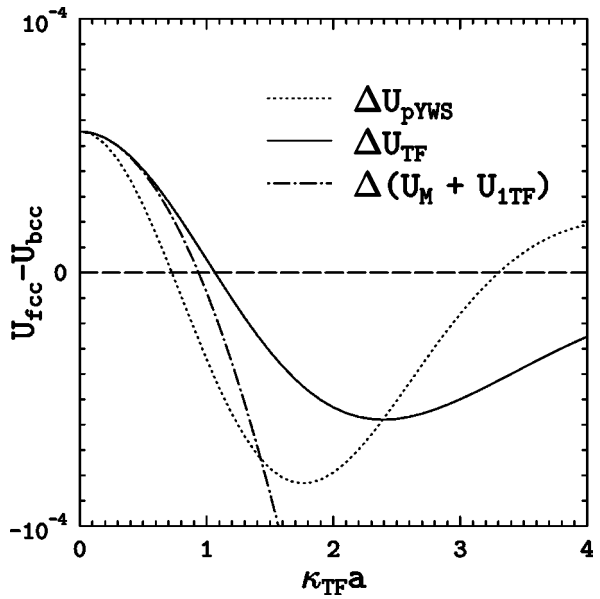

FIG. 2. Energy difference (in units of Z^2e^2/a) between fcc and bcc lattices versus $\kappa_{\mathrm{TF}}a$; ΔU_{TF} (solid line), $\Delta(U_{\mathrm{M}}+U_{1\mathrm{TF}})$ (dash-dotted line), and potential energy difference for YWS (dots).

$$\frac{q^2[\epsilon(q)-1]}{(\kappa_{\mathrm{TF}}a)^2}=\frac{2}{3}-\frac{2}{3}\frac{xy^2}{E}\ln(x+E)+\frac{x^2+1-3x^2y^2}{6yx^2}\ln\left|\frac{1+y}{1-y}\right|+\frac{(2x^2y^2-1)}{6yx^2}\frac{\sqrt{1+x^2y^2}}{E}\ln\left|\frac{yE+\sqrt{1+x^2y^2}}{yE-\sqrt{1+x^2y^2}}\right|, \tag{13}$$

where $x=\hbar k_{\mathrm{F}}/mc$ is the electron relativity parameter determined by the electron number density (or plasma mass density), $E=\sqrt{1+x^2}$, $y=q/2k_{\mathrm{F}}$, and m is the electron mass. Note that the singularity at $y=1$ is actually absent since both the second and the third logarithms are singular and cancel out. Direct summation in Eq. (12) gives the values of η as a function of x shown in Fig. 1 for ten values of $\kappa_{\mathrm{TF}}a$ distributed uniformly in the logarithmic scale between 0.1 and 0.8. At larger $\kappa_{\mathrm{TF}}a$, the linear response approach fails. At larger x, η becomes constant since the screening in the ultrarelativistic electron gas is determined by the only parameter, the ion charge number Z. The latter can be expressed through $\kappa_{\mathrm{TF}}a$ and x via electroneutrality condition as

$$Z=\frac{4}{9\pi}\frac{(\kappa_{\mathrm{TF}}a)^3}{8}\left(\frac{\pi\hbar cx}{e^2E}\right)^{3/2}. \tag{14}$$

Therefore Z is independent of x at large x (since $E\propto x$) and fixed $\kappa_{\mathrm{TF}}a$. We note that due to a complex structure of Eq. (13), η is no longer a constant as in Eq. (10). Comparing Fig. 1 with Eq. (10) one concludes that the TF model at this stage is rather poor and largely overestimates the effect of the electron screening.

It is interesting to compare the static energy of two lattices, bcc and fcc, calculated to first order in $(\kappa_{\mathrm{TF}}a)^2$, $U_{\mathrm{M}}+U_1$. In the rigid electron background, bcc is known to be more tightly bound than fcc: $U_{\mathrm{M,bcc}}<U_{\mathrm{M,fcc}}$, cf. Eq. (8). The same holds true if we use the weak-screening expansion of the TF model, Eq. (9), unless $\kappa_{\mathrm{TF}}a\approx 1$ (dash-dotted curve in Fig. 2). Formally, fcc has lower energy than bcc at larger $\kappa_{\mathrm{TF}}a$ where the linear response formalism becomes invalid. The full TF model, Eq. (5), also predicts the structural transition from bcc to fcc at $\kappa_{\mathrm{TF}}a\approx 1$ (solid line in Fig. 2).

Our calculations show that in the case of realistic RPA screening [Eqs. (11) and (13)], the situation is more sophisticated. For mildly relativistic electron gas ($x\sim 1$), the regions appear in the x-$\kappa_{\mathrm{TF}}a$ plane where the energy of fcc is lower. In Fig. 3, these regions are encircled by the solid lines calculated using the above RPA formalism. The dashed lines show the same contours but are obtained including the effects of zero point ion vibrations as explained in Sec. IV. Dots show lines of fixed charge numbers Z, varying from 1 to 26. Therefore if we compress matter with given chemical composition (given Z) moving along a dotted line from right to left, we can encounter the structural transition. It is remarkable that the transitions occur for selected groups of Z (1; 3, 4; 6, 7; 11–15; 24–26), and do not occur for other Z.

Figures 4 and 5 elucidate the appearance of structural transitions showing oscillations of the difference $(U_{\mathrm{M}}+U_1)_{\mathrm{fcc}}-(U_{\mathrm{M}}+U_1)_{\mathrm{bcc}}$ (dash-dotted line) as a function of x for $\kappa_{\mathrm{TF}}a=0.504$ and 0.8. The dense dotted lines display the difference of Madelung energies, which is always positive. It is important that the absolute value of the energy difference in polarizable electron background can be significantly larger than in the rigid backround OCP.

Let us turn to the energy of YWS. The *potential* energy per ion U_p for a charge distribution described by a dielectric function $\epsilon(q)$ can be calculated exactly as

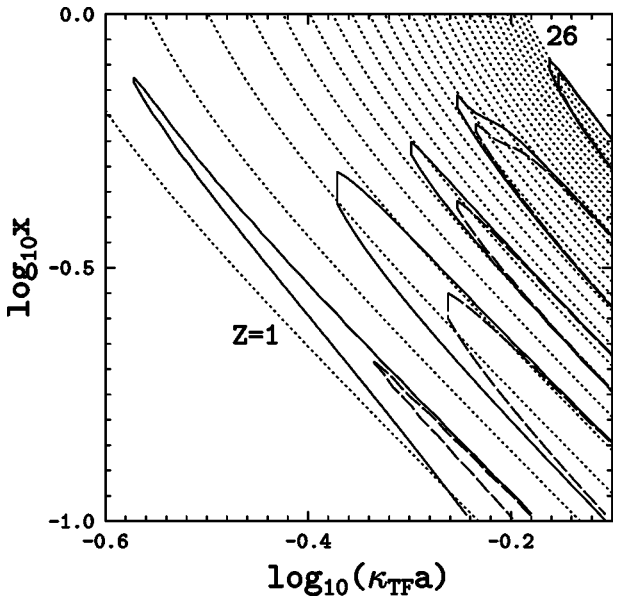

FIG. 3. Contours in the density-compressibility ($x-\kappa_{\mathrm{TF}}a$) plane encircling the domains where fcc lattice has lower energy than bcc at $T=0$. Solid lines represent static lattice energy and the dashed lines represent the effect of zero-point ion motion (for ion mass numbers $A=2Z$). Dots show lines of fixed charge number Z from $Z=1$ to $Z=26$ (from left to right).

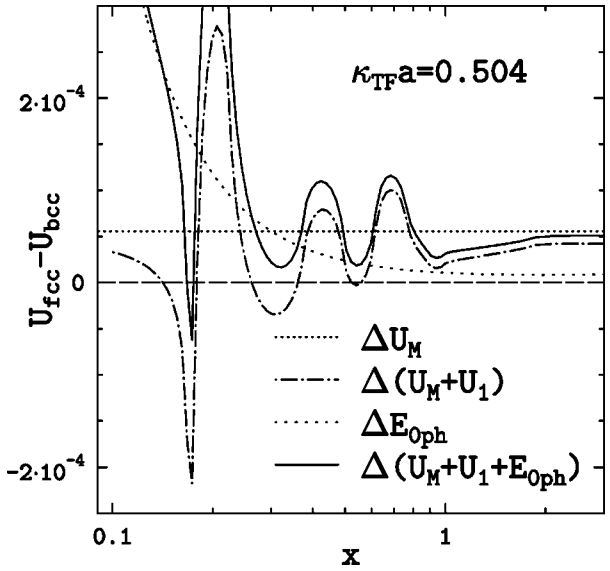

FIG. 4. Difference in energy (in units of Z^2e^2/a) of fcc and bcc lattices versus the density parameter x at $\kappa_{\mathrm{TF}}a=0.504$ and $T=0$. Dense dots show the difference of Madelung energies. Dash-dotted line is the difference of the linear response RPA energies $U_{\mathrm{M}}+U_1$ for static ions. Spaced dots show difference of zero-point energies (Z being uniquely determined by x and $\kappa_{\mathrm{TF}}a$, $A=2Z$). Solid line is the total energy difference including zero-point vibrations. Comparing the solid and dash-dotted lines one sees how the zero-point vibrations eliminate two of the three domains where fcc is energetically preferable for static-lattice ions.

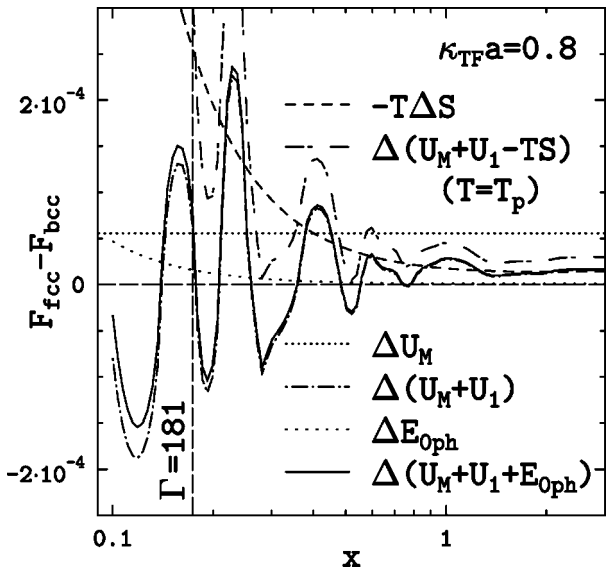

FIG. 5. Difference in free energy (in units of Z^2e^2/a) for $\kappa_{\mathrm{TF}}a=0.8$. Short-dashed and dash-dot-spaced lines correspond to $T=T_p$, the ion plasma temperature, in the approximation of classical ions (Sec. IV). Other curves show the same quantities as in Fig. 4 ($T=0$). Short dashes show the difference of fcc and bcc crystal entropies divided by the ion coupling parameter Γ. Dash-dot-spaced line is the difference of free energies of classical fcc and bcc crystals. Zero-point vibrations do not alter significantly the domains obtained for static-lattice ions (cf. solid and dash-dotted lines). However, heating the crystal to classical temperatures ($T\gtrsim T_p$) completely eliminates the lattice-type transitions and makes bcc lattice thermodynamically preferable at all x. The vertical line approximately corresponds to melting of classical OCP.

$$\frac{U_p}{Z^2e^2}=\frac{1}{2}{\sum_{\mathbf{R}}}'\int\frac{d\mathbf{q}}{(2\pi)^3}\frac{4\pi e^{i\mathbf{q}\cdot\mathbf{R}}}{q^2\epsilon^2(q)}-\frac{1}{2}\int\frac{d\mathbf{q}}{(2\pi)^3}\frac{4\pi}{q^2}\left[1-\frac{1}{\epsilon^2(q)}\right]. \tag{15}$$

For $\epsilon=\epsilon_{\mathrm{TF}}$, Eq. (4), which is the case of YWS, one can again use the Ewald transformation with the result

$$\frac{U_{p\mathrm{YWS}}}{Z^2e^2}={\sum_{\mathbf{R}}}'\left[\frac{1}{4R}(E_++E_-)+\frac{\kappa_{\mathrm{TF}}}{8}(E_+-E_-)\right]+2\pi n{\sum_{\mathbf{G}}}\frac{e^{-A(G^2+\kappa_{\mathrm{TF}}^2)}}{(G^2+\kappa_{\mathrm{TF}}^2)^2}[G^2-A\kappa_{\mathrm{TF}}^2(G^2+\kappa_{\mathrm{TF}}^2)]-\frac{e^{-A\kappa_{\mathrm{TF}}^2}}{2\sqrt{\pi A}}-\frac{3\kappa_{\mathrm{TF}}}{4}\mathrm{erf}(\kappa_{\mathrm{TF}}\sqrt{A}). \tag{16}$$

This formula reproduces Eq. (7) in the limit $\kappa_{\mathrm{TF}}\to 0$. Also the energy difference $\Delta U_{p\mathrm{YWS}}$ between bcc and fcc lattices indicates two lattice-type transitions: from bcc to fcc and from fcc to bcc at $\kappa_{\mathrm{TF}}a\approx 1$ and $\kappa_{\mathrm{TF}}a\approx 3$, respectively (Fig. 2). The dependence $\Delta U_{p\mathrm{YWS}}(\kappa_{\mathrm{TF}}a)$ closely resembles that obtained by Hall [5].

On the other hand, Eq. (15) possesses one important drawback that precludes its use for a real system. It does not include the change in the electron kinetic energy caused by the Coulomb interaction with ions. For this reason if we expand Eq. (16) in terms of $(\kappa_{\rm TF}a)^2$, the first-order term will be $2U_{1\rm TF}$. By contrast, the linear response formula, Eq. (3), includes the change of the electron kinetic energy, which appears to be $-1/2$ of the change in the electrostatic energy for terms of order $(\kappa_{\rm TF}a)^2$.

III. DYNAMICAL MATRIX

Equation (2) gives the energy of the Coulomb system with polarizable background for arbitrary fixed positions of ions, which are not necessarily lattice sites. In the crystal phase, we can take into account the ion motion near lattice sites in the harmonic lattice model. For this purpose, we expand Eq. (2) in powers of ion displacements from the lattice positions **R** and restrict ourselves to the second-order term. This term is a bilinear form with respect to ion displacements. The matrix of this form is the so-called dynamical matrix. Generally, the dynamical matrix can be written in momentum space as [1]

$$D^{\alpha\beta}(\mathbf{q})=\frac{Z^2e^2}{M}\frac{\partial^2}{\partial X_\alpha\partial X_\beta}\Bigg[\sum_{\mathbf{R}}{}'\int\frac{d\mathbf{k}}{(2\pi)^3}\frac{4\pi}{k^2\epsilon(\mathbf{k})}\times e^{i\mathbf{k}\cdot(\mathbf{R}-\mathbf{X})}(1-e^{-i\mathbf{q}\cdot\mathbf{R}})\Bigg]_{\mathbf{X}=0}$$
$$=\omega_p^2\sum_{\mathbf{G}}\left[\frac{(G^\alpha+q^\alpha)(G^\beta+q^\beta)}{(\mathbf{G}+\mathbf{q})^2\epsilon(\mathbf{G}+\mathbf{q})}-\frac{G^\alpha G^\beta}{G^2\epsilon(G)}\right]. \tag{17}$$

In the case of TF screening, one can use the Ewald transformation to derive a formula that speeds up considerably the calculation of the dynamical matrix as compared to direct summation in Eq. (17):

$$D^{\alpha\beta}_{\rm TF}(\mathbf{q})\frac{M}{Z^2e^2}=4\pi n\sum_{\mathbf{G}}\left\{\frac{(G^\alpha+q^\alpha)(G^\beta+q^\beta)}{(\mathbf{G}+\mathbf{q})^2+\kappa_{\rm TF}^2}e^{-A[(\mathbf{G}+\mathbf{q})^2+\kappa_{\rm TF}^2]}-\frac{G^\alpha G^\beta}{G^2+\kappa_{\rm TF}^2}e^{-A(G^2+\kappa_{\rm TF}^2)}\right\}$$
$$+\frac{1}{2}\sum_{\mathbf{R}}{}'\,[1-\cos(\mathbf{q}\cdot\mathbf{R})]\Bigg\{\left[(\kappa_{\rm TF}R-1)E_+-(\kappa_{\rm TF}R+1)E_--\frac{2R}{\sqrt{\pi A}}e^{-A\kappa_{\rm TF}^2-R^2/4A}\right]$$
$$\times\left(\frac{\delta^{\alpha\beta}}{R^3}-\frac{3R^\alpha R^\beta}{R^5}\right)+\left(\kappa_{\rm TF}^2E_++\kappa_{\rm TF}^2E_-+\frac{R}{A\sqrt{\pi A}}e^{-A\kappa_{\rm TF}^2-R^2/4A}\right)\frac{R^\alpha R^\beta}{R^3}\Bigg\}. \tag{18}$$

In the limit $\kappa_{\rm TF}\to 0$, this equation reproduces the well-known expression for the dynamical matrix of the OCP:

$$D^{\alpha\beta}_{\rm OCP}(\mathbf{q})\frac{M}{Z^2e^2}=4\pi n\left[\sum_{\mathbf{G}}\frac{(G^\alpha+q^\alpha)(G^\beta+q^\beta)}{(\mathbf{G}+\mathbf{q})^2}e^{-A(\mathbf{G}+\mathbf{q})^2}-\sum_{\mathbf{G}}{}'\frac{G^\alpha G^\beta}{G^2}e^{-AG^2}\right]$$
$$-\sum_{\mathbf{R}}{}'\,[1-\cos(\mathbf{q}\cdot\mathbf{R})]\left\{\left[\mathrm{erfc}\left(\frac{R}{2\sqrt{A}}\right)+\frac{R}{\sqrt{\pi A}}e^{-R^2/4A}\right]\left(\frac{\delta^{\alpha\beta}}{R^3}-\frac{3R^\alpha R^\beta}{R^5}\right)-\frac{e^{-R^2/4A}}{A\sqrt{\pi A}}\frac{R^\alpha R^\beta}{2R^2}\right\}. \tag{19}$$

Using the dynamical matrix, one can solve the secular equation and find the frequencies of the phonon modes in the Coulomb crystal with polarizable background. For the case of TF screening, Eq. (18) provides a very convenient way to calculate the dynamical matrix. In the general case, one has to separate $D_{\rm OCP}$ from Eq. (17), and then perform direct summation over the reciprocal lattice vectors, which is very time consuming. However, surprisingly, the phonon modes appear to be virtually the same in the cases of TF and RPA screening for all wave vectors **q**. This is illustrated in Figs. 6 and 7. The lines are drawn using the TF dynamical matrix (18). The various symbols show the phonon frequencies calculated using the dynamical matrix (17) with the full RPA dielectric function for three values of electron relativity parameter $x=0.1$,1, and 10. The agreement is very good.

Let us turn to the case of YWS. Taking the energy as a function of ion coordinates as in Eq. (15), we can again calculate the second derivative and obtain the Hamiltonian describing the ion motion in the harmonic lattice approximation. In the general case,

$$D^{\alpha\beta}(\mathbf{q})=\frac{Z^2e^2}{M}\frac{\partial^2}{\partial X_\alpha\partial X_\beta}\Bigg[\sum_{\mathbf{R}}{}'\int\frac{d\mathbf{k}}{(2\pi)^3}\frac{4\pi}{k^2\epsilon^2(\mathbf{k})}e^{i\mathbf{k}\cdot(\mathbf{R}-\mathbf{X})}(1-e^{-i\mathbf{q}\cdot\mathbf{R}})\Bigg]_{\mathbf{X}=\mathbf{0}}$$
$$=\omega_p^2\sum_{\mathbf{G}}\left[\frac{(G^\alpha+q^\alpha)(G^\beta+q^\beta)}{(\mathbf{G}+\mathbf{q})^2\epsilon^2(\mathbf{G}+\mathbf{q})}-\frac{G^\alpha G^\beta}{G^2\epsilon^2(G)}\right]. \tag{20}$$

Furthermore, adopting the TF dielectric function, we can apply the Ewald procedure to the dynamical matrix with the following result:

$$D^{\alpha\beta}_{\mathrm{YWS}}(\mathbf{q})\frac{M}{Z^2e^2}=4\pi n\sum_{\mathbf{G}}\left\{\frac{(G^\alpha+q^\alpha)(G^\beta+q^\beta)}{(\mathbf{G}+\mathbf{q})^2+\kappa_{\mathrm{TF}}^2}e^{-A[(\mathbf{G}+\mathbf{q})^2+\kappa_{\mathrm{TF}}^2]}\right.$$
$$\times\left[1-A\kappa_{\mathrm{TF}}^2-\frac{\kappa_{\mathrm{TF}}^2}{(\mathbf{G}+\mathbf{q})^2+\kappa_{\mathrm{TF}}^2}\right]-\frac{G^\alpha G^\beta}{G^2+\kappa_{\mathrm{TF}}^2}e^{-A(G^2+\kappa_{\mathrm{TF}}^2)}\left[1-A\kappa_{\mathrm{TF}}^2-\frac{\kappa_{\mathrm{TF}}^2}{G^2+\kappa_{\mathrm{TF}}^2}\right]\Bigg\}$$
$$+\frac{1}{2}{\sum_{\mathbf{R}}}'\,[1-\cos(\mathbf{q}\cdot\mathbf{R})]\Bigg\{\left[(\kappa_{\mathrm{TF}}R-1)E_+-(\kappa_{\mathrm{TF}}R+1)E_--\frac{2R}{\sqrt{\pi A}}e^{-A\kappa_{\mathrm{TF}}^2-R^2/4A}\right]$$
$$\times\left(\frac{\delta^{\alpha\beta}}{R^3}-\frac{3R^\alpha R^\beta}{R^5}\right)+\left[\kappa_{\mathrm{TF}}^2E_++\kappa_{\mathrm{TF}}^2E_-+\frac{R}{A\sqrt{\pi A}}e^{-A\kappa_{\mathrm{TF}}^2-R^2/4A}\right]\frac{R^\alpha R^\beta}{R^3}$$
$$+\frac{\kappa_{\mathrm{TF}}^2}{2}\left[\left(\frac{\delta^{\alpha\beta}}{R}-\frac{3R^\alpha R^\beta}{R^3}\right)(E_++E_-)-\frac{2}{\sqrt{\pi A}}\frac{R^\alpha R^\beta}{R^2}e^{-A\kappa_{\mathrm{TF}}^2-R^2/4A}+\frac{\kappa_{\mathrm{TF}}R^\alpha R^\beta}{R^2}(E_+-E_-)\right]\Bigg\}. \qquad (21)$$

In the limit $\kappa_{\mathrm{TF}}\to 0$, the matrix D_{YWS} reproduces D_{OCP}. If we expand D_{YWS} in powers of $(\kappa_{\mathrm{TF}}a)^2$, the term proportional to $(\kappa_{\mathrm{TF}}a)^2$ will be twice the corresponding term in the expansion of D_{TF}. This coefficient has the same origin as the factor 2 in the linear term of the expansion of U_{YWS}. However, the matrix D_{YWS}, Eq. (21), unlike D and D_{TF}, Eqs. (17) and (18), is not positively definite for whatever small values of $\kappa_{\mathrm{TF}}a$ for both bcc and fcc. This indicates that the phonon modes have imaginary frequencies. Accordingly, the bcc and fcc lattice structures of the YWS are unstable, and the question which of them has lower static energy is purely of academic interest.

This point is illustrated in Fig. 8. Shown is the absolute value of the trace of the dynamical matrix of YWS (solid lines) and the trace of D_{TF} (dotted lines). Let us remind that the trace gives the sum of squared eigenfrequencies of all phonon branches. From up to down the lines correspond to decreasing length of the wave vector **q**. The length in units of $\sqrt{3}/a$ is indicated for D_{YWS} and is the same for D_{TF}. The direction of **q** in the reciprocal lattice is $\langle 111\rangle$ (as in Fig. 6). The sharp dips of the solid curves indicate the points where the trace of the dynamical matrix changes sign. One can see

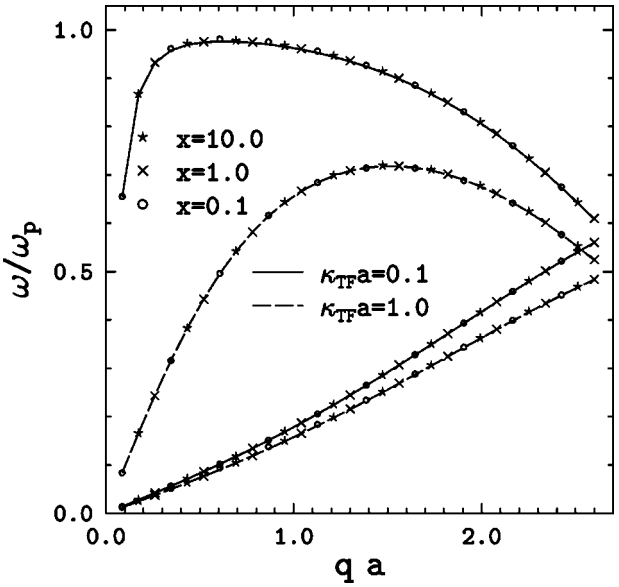

FIG. 6. Eigenfrequencies in a Coulomb crystal with polarizable background ($\kappa_{\mathrm{TF}}a=0.1$ and 1), calculated using the TF model for the dynamical matrix (lines) and the dynamical matrix with the RPA dielectric function (symbols) at $x=0.1$, 1, and 10. The wave vector direction in the fcc lattice (which is reciprocal to bcc) is $\langle 111\rangle$. Because of the high symmetry of this direction, two low-frequency modes have the same dispersion at both values of $\kappa_{\mathrm{TF}}a$.

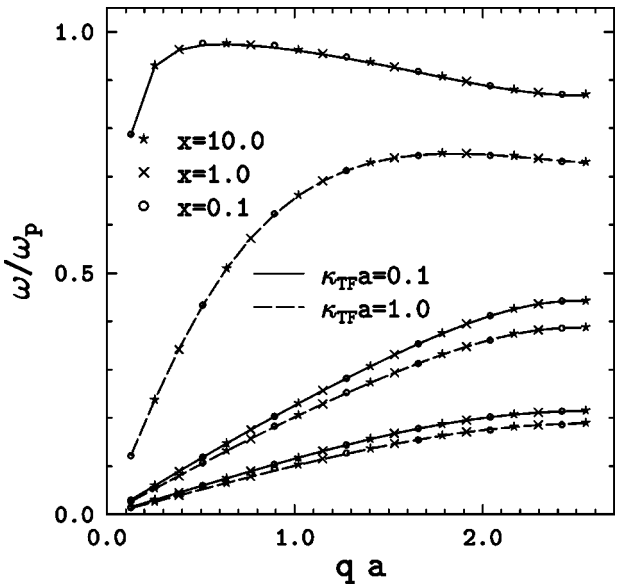

FIG. 7. Same as in Fig. 6, but the direction of the phonon wave vector does not correspond to any symmetry axis of fcc.

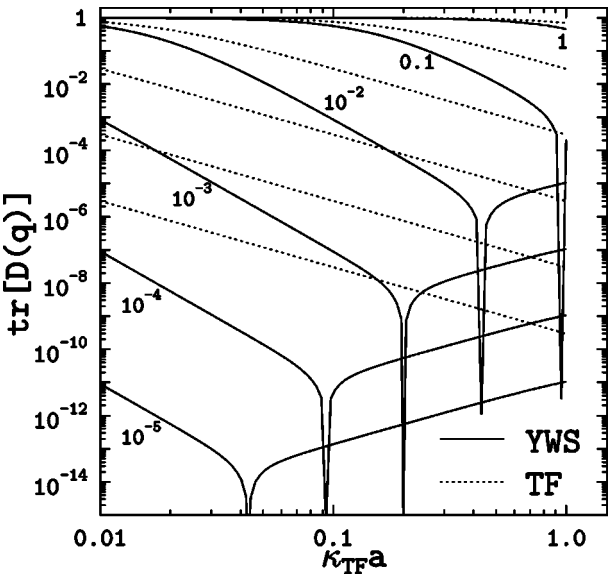

FIG. 8. Absolute values of the trace of dynamic matrix D_{YWS} (solid lines) and the trace of D_{TF} (dashed lines) in units of ω_p^2 for wave vector lengths indicated near the solid curves in units of $\sqrt{3}/a$. Dips correspond to sign reversal of tr(D_{YWS}).

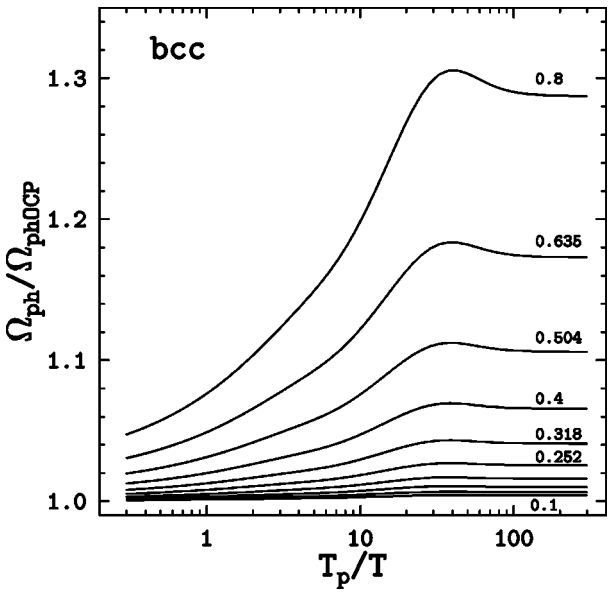

FIG. 9. The ratio of the phonon thermodynamic potential per ion to its value in OCP versus T_p/T for several values of the screening parameter $\kappa_{\mathrm{TF}}a$. The ranges $T_p/T \gg 1$ and $T_p/T < 1$ correspond to the quantum and classical crystals.

that with $\kappa_{\mathrm{TF}} \to 0$, the wavevector at which the instability occurs tends to the center of the Brillouin zone (BZ).

IV. SPECIFIC HEAT

After diagonalization of the dynamical matrix and quantization of the ion motion, we can describe the states of the ion system by numbers of phonons with a certain wave vector **q** and polarization index *s*. In the harmonic approximation, the phonons do not interact and we deal with the thermodynamics of ideal Bose gas of phonons.

All the thermodynamic quantities (per ion) are expressed as derivatives of the thermodynamic potential. The latter can be written as a sum (actually an integral) over the phonon wave vectors **q** lying in the first Brillouin zone:

$$\Omega_{\mathrm{ph}} = -T \sum_{\mathbf{q}s} \ln(1 - e^{-\hbar\omega_{\mathbf{q}s}/T}). \tag{22}$$

For instance, the energy and specific heat are given by

$$E_{\mathrm{ph}} = \Omega - T\left(\frac{\partial\Omega}{\partial T}\right)_{\mu,V} = \sum_{\mathbf{q}s} \frac{\hbar\omega_{\mathbf{q}s}}{e^{\hbar\omega_{\mathbf{q}s}/T} - 1},$$

$$C_{\mathrm{ph}} = -T\left(\frac{\partial^2\Omega}{\partial T^2}\right)_{\mu,V} = \frac{1}{4T^2} \sum_{\mathbf{q}s} \frac{\hbar^2\omega_{\mathbf{q}s}^2}{\sinh^2(\hbar\omega_{\mathbf{q}s}/2T)}. \tag{23}$$

The integration over the Brillouin zone can be done by the method outlined in Ref. [7]. The ratios of the calculated quantities to their values in OCP (according to Refs. [1,8]) are shown in Figs. 9–11 as functions of T_p/T (where T_p is the ion plasma temperature) for the same values of the screening parameter as in Fig. 1. Generally, the modification of the phonon thermodynamic properties due to electron polarizability is seen to be quite moderate ($\lesssim 30\%$).

Figure 12 shows various contributions to the total specific heat of carbon plasma at density $\rho = 10^6\ \mathrm{g\,cm^{-3}}$ ($x = 0.801, \kappa_{\mathrm{TF}}a = 0.425$) as a function of the Coulomb coupling parameter $\Gamma = Z^2e^2/aT$. These conditions are typical for the cores of white dwarfs and envelopes of neutron stars. The dashed curve is the specific heat of degenerate electrons, the curves marked "i" show the phonon specific heat for OCP (dots) and for crystal with polarizable background (solid line). The curves marked "$e+i$" show the total specific heat. The correction due to the polarizable background

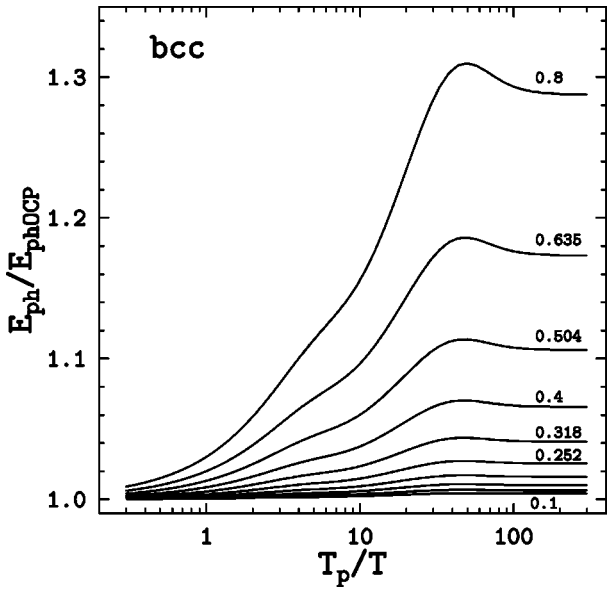

FIG. 10. Same as in Fig. 9 but for phonon thermal energy.

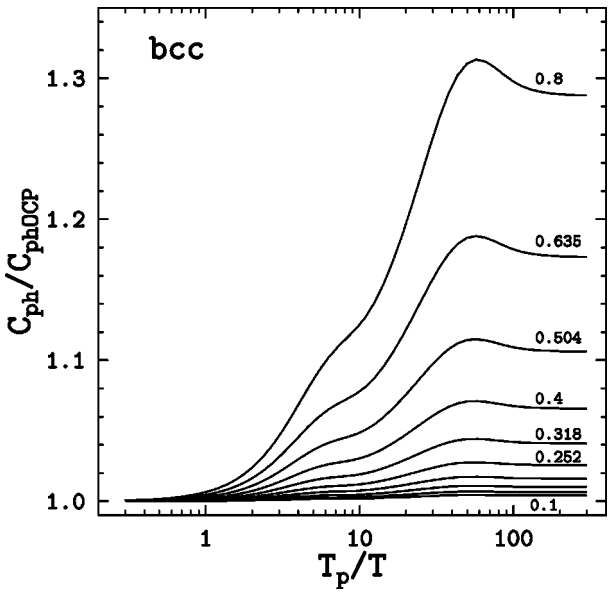

FIG. 11. Same as in Figs. 9 and 10 but for phonon specific heat.

is seen to be positive and is very small. It is clear that phonons give the dominant contribution to the specific heat in the broad range of physical parameters.

Actually, the phonon energy $E_{\rm ph}$ (and the thermodynamic potential) must be complemented by the term $E_{0\rm ph}=1.5\hbar\omega_p u_1$, responsible for zero-point ion vibrations, where u_k is the kth moment of the phonon spectrum:

$$u_k=\langle(\omega_{\mathbf{q}s}/\omega_p)^k\rangle_{\rm ph},$$

$$\langle f(\omega_{\mathbf{q}s})\rangle_{\rm ph}\equiv\frac{1}{3N}\sum_{\mathbf{q}s} f(\omega_{\mathbf{q}s})=\frac{1}{3(2\pi)^3 n}\sum_s\int_{\rm BZ} d\mathbf{q} f(\omega_{\mathbf{q}s}). \tag{24}$$

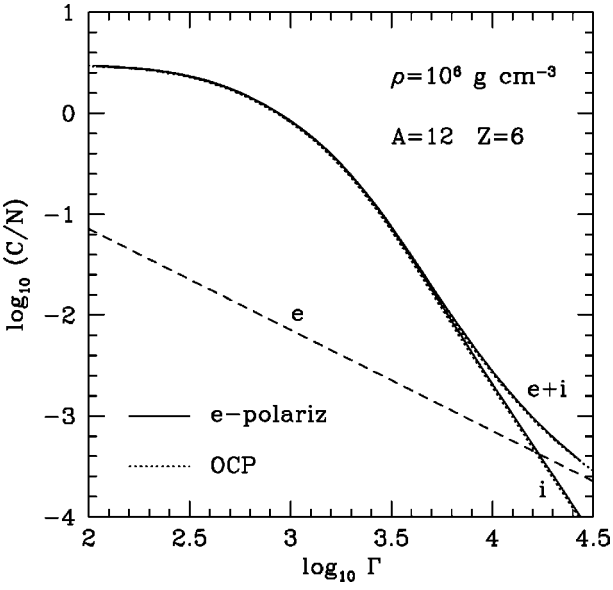

FIG. 12. Various contributions to the specific heat of carbon plasma at $\rho=10^6$ g cm^{-3} as a function of the Coulomb coupling parameter Γ.

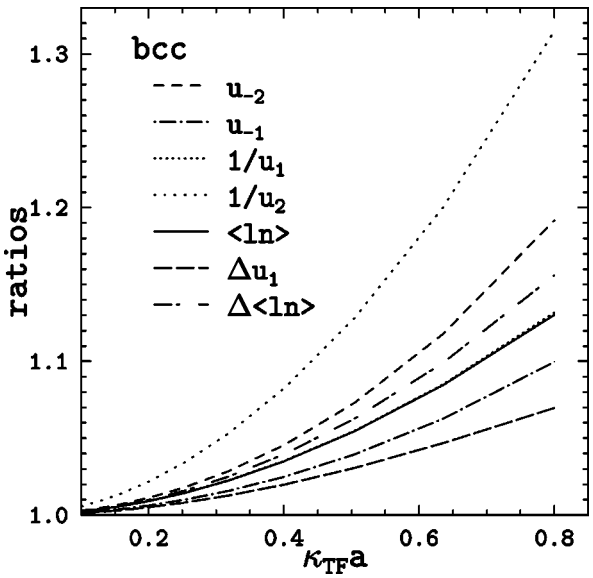

FIG. 13. Ratios of u_{-2}, u_{-1}, u_1^{-1}, u_2^{-1}, $\langle\ln(\omega/\omega_p)\rangle_{\rm ph}$ for the bcc lattice, and of $u_{1,\rm fcc}-u_{1,\rm bcc}$ and $\langle\ln(\omega/\omega_p)\rangle_{\rm ph,fcc}-\langle\ln(\omega/\omega_p)\rangle_{\rm ph,bcc}$ to the values of these quantities for OCP versus the screening parameter.

We have calculated several principal moments u_k in the polarizable electron background. It is convenient to introduce the ratios $u_k/u_{k\rm OCP}$. We have also calculated the ratios of $u_{1,\rm fcc}-u_{1,\rm bcc}$ and $\langle\ln(\omega/\omega_p)\rangle_{\rm ph,fcc}-\langle\ln(\omega/\omega_p)\rangle_{\rm ph,bcc}$ to the values of these quantities in OCP. These ratios are shown in Fig. 13. The moments u_{-2} and u_{-1} determine the classical and quantum asymptotes of the ensemble average rms ion displacements from the lattice positions; $u_2=1$ for OCP (Kohn sum rule), but deviates from this value in the polarizable background; $\langle\ln(\omega/\omega_p)\rangle_{\rm ph}$ is important for classical asymptote of the crystal entropy. The differences between u_1's and $\langle\ln(\omega/\omega_p)\rangle_{\rm ph}$'s for fcc and bcc are important for comparing the free energies of these lattices in the quantum and classical regimes, respectively (see below).

With high precision (maximum error $<0.05\%$ for $\kappa_{\rm TF}a\leqslant 0.8$), all these ratios can be fitted as

$$1+p_1(\kappa_{\rm TF}a)^2+p_2(\kappa_{\rm TF}a)^4+p_3(\kappa_{\rm TF}a)^6. \tag{25}$$

The OCP values and fit parameters are given in Table I.

Let us note that the solid contours in Fig. 3 and the dash-dotted lines in Figs. 4 and 5 were calculated by neglecting displacements of ions from their lattice sites. Actually, the ions are smeared around their positions in the static lattice due to thermal and zero-point vibrations. The vibrations are different for bcc and fcc, which affect the position of structural transitions (contours in Fig. 3) between these lattices. In the quantum $T=0$ limit, the transitions are determined by zeros of the energy difference. To include the ion vibrations in this case, we have added the difference in zero-point energy $1.5\hbar\omega_p\Delta u_1$ to the difference $\Delta(U_{\rm M}+U_1)$. The zero-point energy difference is shown in Figs. 4 and 5 by spaced dots, assuming the ion mass number $A=2Z$, while Z is determined uniquely by $\kappa_{\rm TF}a$ and x. The total zero-temperature energy difference is shown by solid line. It is seen that at

TABLE I. Moments for zero screening and values of the fitting parameters.

	$\kappa_{\mathrm{TF}}a=0$	p_1	p_2	p_3
u_{-2}	12.973	0.2789217	0.03209666	0
u_{-1}	2.7986	0.1548433	0.001007932	0
$1/u_1$	1/0.5113875	0.2290487	-0.06287747	0.04113361
$1/u_2$	3	0.5406582	-0.1802477	0.1639836
$\langle\ln(\omega/\omega_p)\rangle_{\mathrm{ph}}$	-0.831298	0.2236195	-0.03940911	0.01198610
Δu_1	0.0018065	0.1325671	-0.05446109	0.02705265
$\Delta\langle\ln(\omega/\omega_p)\rangle_{\mathrm{ph}}$	0.01339	0.2503483	-0.02134253	0.01733280

$\kappa_{\mathrm{TF}}a=0.504$, the zero-point energy difference eliminates two of the three domains where fcc is preferable for static lattice. By contrast, at $\kappa_{\mathrm{TF}}a=0.8$, the zero-point energy difference leads only to minor shifts of the structural transition positions. In Fig. 3, the positions of the structural transitions with account of zero-point energy are shown by dashes. The domains shrink a little at high Z, while at low Z the domains change significantly, indicating the importance of zero-point vibrations for lighter ions.

In the classical limit $T>T_p$, the structural transition is determined by the zeros of the free energy $F=E-TS$, where S is the entropy. If $T\ll T_{\mathrm{F}}$, where T_{F} is the Fermi temperature of electrons, then the static lattice part of E is the same as at $T=0$. The phonon energy in the classical limit is identical for both lattices being equal to $3T$; the zero-point terms cancel out. The difference in classical entropy reads $-3\Delta\langle\ln(\omega/\omega_p)\rangle_{\mathrm{ph}}$. Thus the position of the structural transitions is determined by zeros of $\Delta[U_{\mathrm{M}}+U_1+3T\langle\ln(\omega/\omega_p)\rangle_{\mathrm{ph}}]/T\Gamma$. The differences in $-\Delta S/\Gamma$ and in $\Delta F/T\Gamma$ between fcc and bcc are shown in Fig. 5 by short dashes and dash-dot-spaced line, respectively. The temperature is set equal to T_p and the classical limit of S is assumed. The vertical line, $\Gamma=181$, represents approximately the phase transition from liquid to solid in the classical OCP. We see that heating matter to $T\gtrsim T_p$ completely eliminates the domains where fcc is thermodynamically preferable at $T=0$.

Our conclusion about the smallness of the polarization corrections to various phonon thermodynamic quantities in a Coulomb solid in a broad range of temperatures and densities contradicts that obtained by Potekhin and Chabrier [4] (cf. Fig. 8 and Sec. 6 in Ref. [4]). The reason for the discrepancy can be twofold. First, the thermodynamic quantities were evaluated in Ref. [4] using the perturbation theory, whereas the results presented in this work are based on the accurate calculation of the phonon spectrum of a Coulomb solid with compressible electron background. The authors of Ref. [4] realized that their perturbation analysis might have been invalid in the quantum regime of low temperatures, i.e., $T_p/T>1$, where the largest discrepancy with our results occurs. Second, the present calculations are based purely on the harmonic lattice theory, while the results of Ref. [4] by construction contain some (but not all even in the lowest order) anharmonic terms. Although it is unexpected that the anharmonic terms (with or without polarization corrections) can account for the dominant contribution to the thermodynamic quantities at low temperatures, this point deserves an additional investigation.

V. CONCLUSIONS

We have studied the properties of Coulomb solids with realistic polarizable electron background. The TF approximation for electron screening is shown to overestimate significantly the correction to the static lattice energy due to background polarizability as compared to more realistic RPA description of screening (Fig. 1). Once the polarizability of the background is taken into account, the fcc lattice appears to be thermodynamically preferable to bcc at low temperatures (both for static lattice and with zero-point ion motion included, Figs. 3 and 4) for moderately relativistic electrons $x\lesssim 1$ at specific values of the charge number. In the classical regime $T>T_p$, this effect disappears and bcc lattice is preferable in the entire range of physical parameters (Fig. 5). The ion motion in the solid phase is studied using harmonic lattice approximation. It is shown that the dispersion of phonon modes is described very accurately in the TF approximation (Figs. 6 and 7). The latter allows one to use the Ewald method for calculation of the dynamical matrix, which speeds up considerably calculations that involve integration over the phonon modes. Various phonon thermodynamic quantities are calculated. It is shown that electron polarizability leads to only moderate increase of the phonon thrmodynamic quantities (Figs. 9–11) as compared to the case of rigid background. The related model of Yukawa–Wigner Solid is briefly analyzed. This model does not take into account modification of the electron kinetic energy due to electron gas polarizability. As a result, both bcc and fcc lattices appear to be unstable (phonon modes acquire imaginary frequencies).

ACKNOWLEDGMENTS

The author is grateful to D. G. Yakovlev, who suggested the topic of this research, expressed constant interest in this work, proposed numerous improvements to the paper, and obtained the fitting expression (25). The author thanks A. Y. Potekhin for interesting discussions.

[1] E.L. Pollock and J.P. Hansen, Phys. Rev. A **8**, 3110 (1973).
[2] D.G. Yakovlev and D.A. Shalybkov, Sov. Sci. Rev. **7**, 311 (1989).
[3] G. Chabrier and A.Y. Potekhin, Phys. Rev. E **58**, 4941 (1998).
[4] A.Y. Potekhin and G. Chabrier, Phys. Rev. E **62**, 8554 (2000).
[5] G.L. Hall, J. Math. Phys. **24**, 209 (1983).
[6] B. Jancovici, Nuovo Cimento **25**, 428 (1962).
[7] R.C. Albers and J.E. Gubernatis, LASL LA-8674-MS, 1981 (unpublished).
[8] D.A. Baiko, A.Y. Potekhin, and D.G. Yakovlev, Phys. Rev. E **64**, 057402 (2001).